Chemically-powered swimming and diffusion in the microscopic world

Yifei Zhang[1,2†] & Henry Hess[3†]

[1]Beijing Advanced Innovation Center for Soft Matter Science and Engineering, Beijing University of Chemical Technology, Beijing, China
[2]State Key Laboratory of Chemical Resource Engineering, Beijing University of Chemical Technology, Beijing, China
[3]Department of Biomedical Engineering, Columbia University, New York, NY, United States
[†]Email: yifeizhang@mail.buct.edu.cn; hhess@columbia.edu

Abstract | The past decade has seen intriguing reports and heated debates concerning the chemically-driven enhanced motion of objects ranging from small molecules to millimetre-size synthetic robots. These objects, in solutions in which chemical reactions were occurring, were observed to diffuse (spread non-directionally) or swim (move directionally) at rates exceeding those expected from Brownian motion alone. The debates have focused on whether observed enhancement is an experimental artefact or a real phenomenon. If the latter were true, then we would also need to explain how the chemical energy is converted into mechanical work. In this Perspective, we summarize and discuss recent observations and theories of active diffusion and swimming. Notably, the chemo-mechanical coupling and magnitude of diffusion enhancement are strongly size-dependent and should vanish as the size of the swimmers approaches the molecular scale. We evaluate the reliability of common techniques to measure diffusion coefficients and finish by considering the potential applications and chemical-to-mechanical energy conversion efficiencies of typical nano- and microswimmers.

[H1] Introduction

Developing microscopic or nanoscopic machines that convert chemical energy into mechanical work or kinetic energy is an appealing but challenging task that lies at the intersection of synthetic chemistry, synthetic biology and nanotechnology.[1-4] The tiny/minuscule machines that perform work such as dragging,[5] drilling,[6] stirring[7] and delivering cargo[8] are also referred to as nanomotors or micromotors, depending on their sizes. Nature has evolved multiple sophisticated protein-based motors such as myosins, kinesins, dynein, ATP synthase, the ribosome and the flagellar motor. However, the elaborate protein folding, subtle interactions, and highly-ordered architectures of these motors are yet to be fully understood, which prevents the de novo fabrication of synthetic mimics with the same performance. Alternatively, scientists have tried to fabricate motors with similar functions through one of two approaches: synthesizing special molecules with rotatable chemical or mechanical bonds or repurposing biological building blocks (protein motors, enzymes, biological assemblies or even cells) for new applications.[9] Examples of the first approach include alkene-based rotary motors[10] and catenane- or rotaxane-based linear motors[11], the discoveries of which were honored with the 2016 Nobel Prize in Chemistry. The second approach can feature F_1-ATPase enabling rotation of actin filaments[12] or inorganic nanorods[13], kinesin propelling molecular shuttles[14,15] or sperm cells driving microrobots[16], to name but a few examples. Recently, a series of investigations suggested that common small-molecule

reactants,[17,18] as well as enzymes[19-21] and enzyme-coated nano- or microstructures,[22,23] can also be considered motors because their diffusion (and in some cases, the diffusion of the surrounding solvent molecules as well) is enhanced as a consequence of associated chemical reactions. However, the origin, magnitude and potential applications of this phenomenon have been hotly debated over the past five years.

Despite their structural and functional diversity, microscopic and nanoscopic motors encounter a common challenge of propelling themselves in the laminar flow regime and in the presence of strong thermal fluctuations. Purcell's scallop theorem suggests that a micromotor in laminar flow cannot gain any net displacement when undergoing reciprocal motion.[24,25] Furthermore, on the microscale, inertia becomes negligible while viscous forces dominate, such that a swimmer comes to a complete stop soon after propulsion ceases — within microseconds for a 1 μm particle and picoseconds for a 1 nm particle. As the size of a motor decreases, Brownian motion introduces increasingly large fluctuations in position and orientation, which can break the reciprocity of flapping motions[26] but also randomizes directed propulsion. A spherical particle in solution simultaneously undergoes translational and rotational diffusion, and its translational (D_0, Fig. 1a) and rotational diffusion coefficients (D_r) can be described by the Einstein relations (eqs 1,2):

$$D_0 = \frac{k_B T}{6\pi\eta R} \quad (1)$$

$$D_r = \frac{k_B T}{8\pi\eta R^3} = \tau_r^{-1} \quad (2)$$

where k_B is the Boltzmann constant, T is temperature (such that k_BT represents thermal energy), η is the viscosity of the solution, R is the effective hydrodynamic radius of the particle and τ_r is the characteristic rotational relaxation time. When motion is projected into two dimensions, the mean-squared displacement ($<\boldsymbol{x}^2>$, MSD) over a time period Δt is (eq. 3):[27]

$$< \boldsymbol{x}^2 > = 4D_0\Delta t + \frac{v^2\tau_r^2}{2}\left[\frac{2\Delta t}{\tau_r} + e^{-\frac{2\Delta t}{\tau_r}} - 1\right] \quad (3)$$

When $\Delta t << \tau_r$, this simplifies to (eq. 4):

$$< \boldsymbol{x}^2 > = 4D_0\Delta t + v^2\Delta t^2 \quad (4)$$

In the opposite case of $\Delta t >> \tau_r$, we instead get (eq. 5):

$$< \boldsymbol{x}^2 > = (4D_0 + v^2\tau_r)\Delta t = (4D_0 + \frac{l^2}{\tau_r})\,\Delta t \quad (5)$$

where $l = v\tau_r$ is the average persistence length of the ballistic motion. By defining the diffusion enhancement $\Delta D = l^2/4\tau$, this also simplifies to (eq. 6):

$$< \boldsymbol{x}^2 > = (4D_0 + 4\Delta D)\Delta t \quad (6)$$

We see that the MSD of a self-propelled particle scales linearly with Δt at the very beginning, then scales quadratically and finally scales linearly again as the observation time Δt greatly exceeds τ_r. Scaling the MSD by the particle diameter $2R$, Δt by τ_r, and the swimming velocity v by $v^0 = 2R/\tau_r$ gives a dimensionless description of MSD (Fig. 1b)[28]. For a particle to be considered a motor, it must exhibit substantial movement beyond Brownian motion, which is the case when the velocity v resulting from self-propulsion exceeds the ratio of swimmer radius and rotational relaxation time.

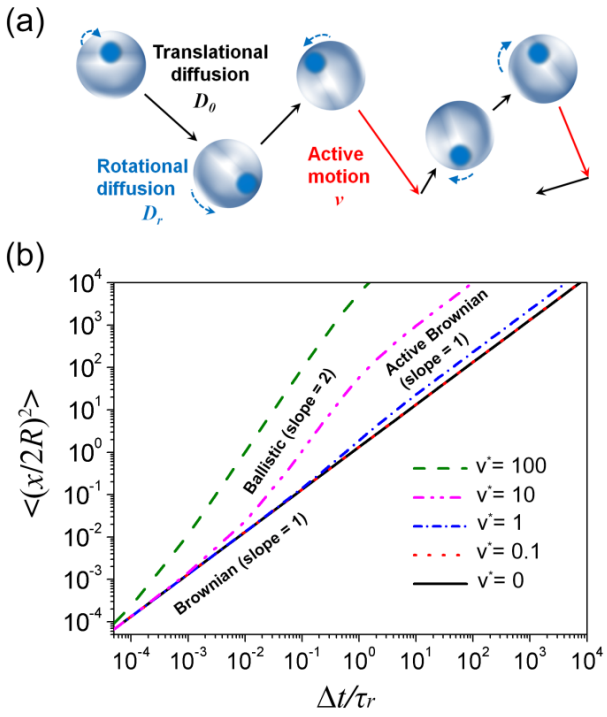

Fig. 1 | **Passive and active motion of a particle. a** | An asymmetric particle can exhibit boosted diffusion in the form of translational diffusion with diffusion coefficient D_0, rotational diffusion with diffusion coefficient D_r, and concurrent active motion with velocity v. **b** | The dimensionless mean-square displacement $<(\boldsymbol{x}/2R)^2>$ (displacement scaled by the swimmer diameter $2R$) as a function of the dimensionless time $\Delta t/\tau_r$ (time scaled to the rotational relaxation time τ_r) for different dimensionless velocities $v' = v\tau_r/2R$ (velocity scaled by the quotient of τ_r to diameter $2R$), as given by Equation 3.

If we consider a particle of size $2R$ = 10 μm, for which τ_r = 10 min in H_2O at room temperature would be typical, it is best to describe MSD over the course of seconds because observations over this timescale will capture ballistic velocity (eq. 4). For a much smaller particle ($2R$ < 10 nm) with τ_r < 1 μs, directional motion is quickly randomized by particle tumbling, such that the particle exhibits apparently enhanced diffusion (eqs 5,6). The diffusive behaviour of a particle of size in between these two regimes depends on complex factors including particle shape and the frequency and magnitude of the propulsive force, leading to a

complicated time-dependent MSD. In practice, a nonlinear dependence may be found as $\langle \boldsymbol{x}^2 \rangle \sim \Delta t^{\alpha}$, where $1 < \alpha < 2$. We now depict some representative chemically-driven microscopic or nanoscopic particles categorized by the above two regimes of MSD (Table 1).

Table 1 | **Experimental observations of self-propelled particles quantified by Equation 4 or 6.**

Swimmer	Size (nm) [a]	Propelled by	D_0 ($\mu m^2 s^{-1}$)	D^*_{max} ($\mu m^2 s^{-1}$) [b]	v ($\mu m s^{-1}$)	Ref
Urease	14	Urea hydrolysis @ urease	31.8	40.6	–	19
Pt–Au Janus NPs	30	H_2O_2 decomposition @ Pt	10.2	12.7	–	29
Pt–Pt–Au Janus NPs	60		6.8	8.9	–	
Janus hollow mesoporous silica nanoparticles	400	H_2O_2 decomposition @ catalase	0.75	1.30	–	23
		Urea hydrolysis @ urease	0.72	1.10	–	
		Glucose oxidation @ GOx	0.72	1.04	–	
Enzyme-coated polystyrene microparticles	790	Decomposition @ catalase	0.8	0.95	–	30
		Urea hydrolysis @ urease	0.67	0.82	–	
	2000	H_2O_2 decomposition @ catalase	0.235	0.245	–	
HRP and cyt *c* modified polypyrrole–Au nanorods	260 × 1700	O_2 oxidization of hypoxanthine @ xanthine oxidase	0.45	0.58	–	31
Pt-nanoparticle-filled polymeric stomatocytes with an opening	300	H_2O_2 decomposition @ Pt NPs	15 [c]	–	23	32
AuPt nanorods	370 × 2000	H_2O_2 decomposition @ Pt NPs	0.4	–	8	33
Polymeric stomatocytes	500	H_2O_2 decomposition @ catalase	9 [c]	–	60	34
		Glucose	9 [c]	–	11	

		oxidation @ catalase and GOx				
Janus hollow mesoporous silica microparticles	2300	Urea hydrolysis @ urease	0.2 [c]	–	10	35
Bacteria attached polystyrene microbeads	10 μm	*Serratia marcescens* metabolism	0.04 [c]	–	1.81 (non-chemotactic)	36
				–	3.29 (chemotactic)	
Natural tissue of radish	1 mm × 7 mm	Catalase and peroxidase	–	–	5	37
		Modified with external catalase	–	–	20	
Conductive C fibres	7 μm × 0.5–1 cm	O_2 oxidization of glucose @ GOx and BOD	–	–	10^4 [d]	38

[a]Spherical particles are described by their diameters and cylindrical particles by their diameter×length. Units are nm unless otherwise stated.
[b]D^*_{max} is the maximum diffusion coefficient observed in the corresponding references.
[c]Estimated based on swimmer size.
[d]At the air–H_2O interface.
BOD, bilirubin oxidase; cyt, cytochrome; GOx, glucose oxidase; HRP, horseradish peroxidase; NP, nanoparticle.

In this Perspective, we focus on chemically-powered swimming or diffusion of microscopic objects in aqueous solution. Based on the sizes of the swimmers, we categorize recent observations into three groups: microparticles ranging in size from hundreds of nanometres to several micrometres, nanoparticles or enzymes ranging in size from a few to tens of nanometres, and small molecules of subnano- to nanoscale dimensions. We review the origins of enhanced motion as well as the controversies associated with it, and also the occasionally observed enhanced transport of tracer particles surrounding active swimmers. The controversies often relate to the accuracy and precision with which one measures diffusion coefficients, so we discuss the reliability of common methods including particle tracking, fluorescence correlation spectroscopy (FCS), dynamic light scattering (DLS) and diffusion nuclear magnetic resonance (NMR) spectroscopy. The potential applications and the chemical-to-mechanical energy conversion efficiency of active swimmers are also surveyed.

[H1] Self-propelled microswimmers

Bimetallic rods can be considered the original systems for self-propelled motion on the microscale.[39] These were followed by Janus particles and enzyme-coated microbeads that are

in the range of hundreds of nanometres to a few micrometres in size. Such microswimmers are most commonly actuated by electrophoresis, diffusiophoresis and bubble ejection.

[H2] Electrophoretic mechanism

Bimetallic microswimmers that directionally locomote in H_2O_2 solutions are primarily driven by electrophoresis in a self-generated electric field.[29,40] The oxidation of H_2O_2 at the anode produces protons ($H_2O_2 \rightarrow O_2 + 2H^+ + 2e^-$), while reduction of H_2O_2 at the cathode consumes protons ($H_2O_2 + 2H^+ + 2e^- \rightarrow 2H_2O$), establishing around the bimetallic swimmer a local electric field that points from the cathode to the anode (Fig. 2a). In turn, this self-generated electric field drives electrophoretic migration of the charged swimmer at a velocity typically in the range of several to hundreds of μms^{-1}. Such a self-electrophoretic mechanism can also propel 2 μm polypyrrole–Au rods with the two ends decorated with different haem enzymes for H_2O_2 decomposition,[41] or in an inverted configuration to establish a bimetallic membrane.[42] The principal problem with this propulsion mechanism is that the H^+ current and the attendant fluid flow are confined to a space a few nanometres from the surface, such that extremely high shear is established near the no-slip surface, leading to high frictional losses.

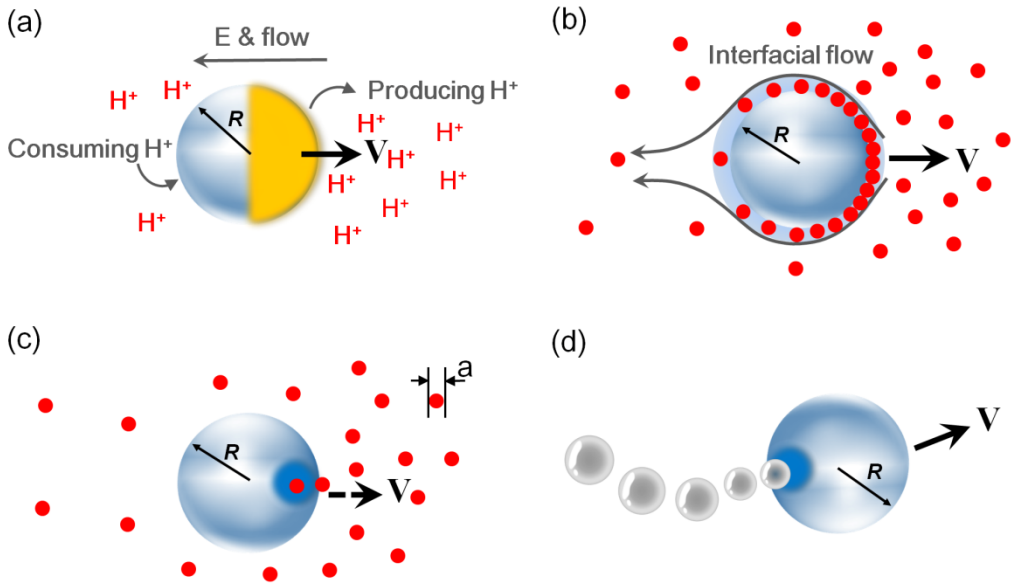

Fig. 2 | **Self-propulsion mechanisms of enhanced diffusion. a** | Electrophoresis of a Janus particle driven by a self-produced [H^+] gradient, for example from concomitant reduction and oxidation of H_2O_2 at the blue and yellow hemispheres, respectively. **b** | Diffusiophoresis of a non-reactive particle in response to an imposed concentration gradient of solute molecules (drawn in red). **c** | Diffusiophoresis of a catalytic particle that produces an anisotropic distribution of products. **d** | Bubbles can propel a particle in the opposite direction to bubble travel.

[H2] Diffusiophoretic mechanisms

Diffusiophoresis of microparticles is caused by a concentration gradient of solutes or solvents — a chemical potential gradient.[43] The motion is driven by a diffusioosmotic slip flow at the particle–fluid interface (Fig. 2b) and the typical migration velocity is on the order of 0.1–10

μms^{-1}.[44,45] For example, solutions with NaCl concentration gradients can see polystyrene particles diffuse at up to 1 μms^{-1}, in proportion to the gradient of the logarithm of electrolyte concentration. The concentration gradients can be externally imposed or can result from salt dissolution, solute crystallization, diffusive mixing or even chemical reactions.[44,45] Among these, reaction-induced self-diffusiophoresis is of particular interest as it enables micro-/nanoscale objects to autonomously swim by generating local concentration gradients in the environment (Fig. 2c).[46]

A crude estimate of the particle motion resulting from the production of a molecule near the catalytic site (Fig. 2c) can be made by considering the osmotic pressure of the molecule on the particle while the molecule is still on one side and near the particle. If the volume occupied by the molecule 'on one side and near the particle' is taken to be similar to that of the particle, the osmotic pressure is given by $p \cong k_BT/V \approx k_BT/(2R)^3$. The resulting force $F = p\pi R^2$ on the particle over time $t \cong 4R^2/D_a = 24\pi\eta aR^2/k_BT$ is limited by the diffusive motion of the molecule away from that side. This force is opposed by the viscous drag on the particle $F = 6\pi\eta Rv$, which moves a distance $vt = (\pi/2)a \cong a$. This estimate indicates that each reaction event that consumes or produces a molecule (occurring at frequency k) can lead to a displacement similar to the size of the substrate (or product) molecule, yielding a swimming velocity $v = ak$ independent of the size of the particle or the viscosity of the solution if the molecules are generated at a specific active site. For a 1 μm particle with a characteristic rotational relaxation time of 1 s, a turnover frequency of 10^3 s^{-1} could propel the particle to migrate a distance comparable to that caused by Brownian motion. Indeed, using a faster reaction or incorporating a higher spatial density of catalytic active sites aids active diffusion in experiments. However, the rapid rotational diffusion of small particles such as enzymes of size ~10 nm requires a turnover frequency exceeding 10^7 s^{-1} to manifest enhanced diffusion. This value of k exceeds the catalytic capacity of most enzymes. Immobilising enzymes (or other catalytic components) on microparticles is a proven strategy to fabricate self-propelled micromotors because it maximizes the turnover events by employing multiple 'engines'. At the same time, having a larger, μm-scale 'body' leads to the desired reasonably slow rotational diffusion. As has been demonstrated experimentally, only micromotors coated with fast enzymes, such as urease and acetylcholinesterase, show diffusion enhancement.[47] Having an asymmetrical distribution of active sites on a particle is also crucial to the effectiveness of this type of micromotors.[48]

[H2] Bubble propulsion

Pioneering work has described how a millimeter-size polydimethylsiloxane 'boat' performs Pt-catalysed H_2O_2 decomposition to power its swimming at a liquid–air interface.[49] Later efforts include the construction of differently-shaped motors (such as rods,[50] tubules,[51] Janus spheres[52] and hollow particles with openings[53]) and the exploitation of new propellants (such as bimetallic alloys, catalytic metal or metal oxide particles,[54] metals that evolve H_2 from H_2O or acids,[55] enzymes[56] or enzyme cascades[34,57]). We classify diverse micromotors into three categories based on the fuels that they consume: H_2O_2, metals and biomolecules such as glucose. H_2O_2-fueled motors have been extensively studied and a relatively high concentration of H_2O_2 is required to sustain a reasonable swimming speed, which severely

limits their biomedical applications. The first metal-fueled motors were Janus microspheres partially coated with an Al−Ga alloy that reacts with H_2O and produces H_2.[55] Later came Zn-based and Mg-based counterparts that could self-propel in the stomach or gastrointestinal tract, greatly advancing their application in drug delivery.[8,58,59] These motors have a limited supply of metal on board and do not need to harvest fuel from their surroundings. Lastly, biomolecule-fueled reactions can enable micromotors to operate by harvesting fuel molecules (such as glucose, ATP and O_2) under physiological conditions. For example, bowl-shaped nanoreactors with compartmentalized cascade enzyme systems consume glucose and phosphoenolpyruvate and exhibit enhanced motion as a result.[34,57] Using enzyme cascade reactions greatly expands the scope of fuel molecules and will help in vivo applications of synthetic micromotors. Modifying the surface of a swimmer to allow for bubbles to form and detach faster can effectively increase the propulsion speed,[60] which typically is in the range 1–1000 μms^{-1}.[61] This is entirely plausible based on a back-of-the-envelope calculation of swimming speed. Assuming, as is often observed,[51,53] that bubbles are roughly equal in radius to the swimmer and each bubble propels the swimmer by $2R$, the swimming velocity v is given by $v = kk_BT/2R^2p$, where k is the rate of production of gas molecules and p is the pressure in the bubble (approximately equal to atmospheric pressure). Note that the displacement per gas molecule produced $k_BT/2R^2p$ multiplied by the Stokes drag of the particle $6\pi\eta R$ yields the work done per reaction, which can reach a substantial fraction of the chemical energy consumed for particles smaller than 1 μm. Unfortunately, bubble formation competes against dissolution of gas molecules into the surrounding solvent, a process which prevents the formation of bubbles at the slow reaction rates typical for smaller swimmers.

[H1] Enhanced diffusion of enzymes and nanoparticles

If we move from microscale particles to smaller swimmers (diameter < 100 nm), we now find that ballistic motion is quickly randomized by rotation, resulting in Brownian-type diffusion with greater diffusion coefficients (Fig. 1b). A variety of enzymes and nanoparticles have been reported to diffuse faster when a reaction is occurring but the underlying mechanisms and even the observations themselves are still under discussion. In this section, we consider catalysis-induced enhanced diffusion as well as the non-catalytic case.

[H2] Catalysis-induced enhanced diffusion of enzymes and nanoparticles

Proteins and nanoparticles from several to tens of nanometres in size play a crucial role in converting molecular events into macroscopic functionalities. For instance, highly-evolved protein motors such as kinesin and ATP synthase efficiently perform mechanical work by coupling a catalytic cycle to a cycle of mechanical motion. It is natural to ask whether other enzymes could also use a portion of free energy from their catalytic reactions to power their locomotion (Fig. 3a). Measurements by Sen's group first indicated that the diffusion coefficient of urease increased by 16–28% in the presence of its substrate urea.[19] Such an increase seemed to follow a Michaelis–Menten-like dependence on [urea]. Following this example, other enzymes, including catalase,[21] alkaline phosphatase,[21] acetylcholinesterase,[62] hexokinase[63] and even the endothermic aldolase,[64] were examined by different groups and shown to have similar magnitudes of diffusion enhancement. These results quickly sparked hot debates, which initially focused on the origin of enhancement but ended up with mounting

contradictory claims that are difficult to reconcile.[62,64-70] Theoretical calculations suggested that the effect of diffusion enhancement should be much smaller than had been measured using FCS. Indeed, to increase the diffusion coefficient by 30%, the stroke size of an enzyme would have to be an order of magnitude larger than its hydrodynamic radius.[71] Moreover, the energy released from common enzymatic reactions is insufficient to sustain the diffusion enhancement.[72] Although conformational changes of an enzyme can lower its hydrodynamic radius and lead to higher diffusivity without the need of additional energy consumption, the corresponding shrinkage is typically less than 5%, which is far from what is necessary for the apparent 30% enhancement.[73]

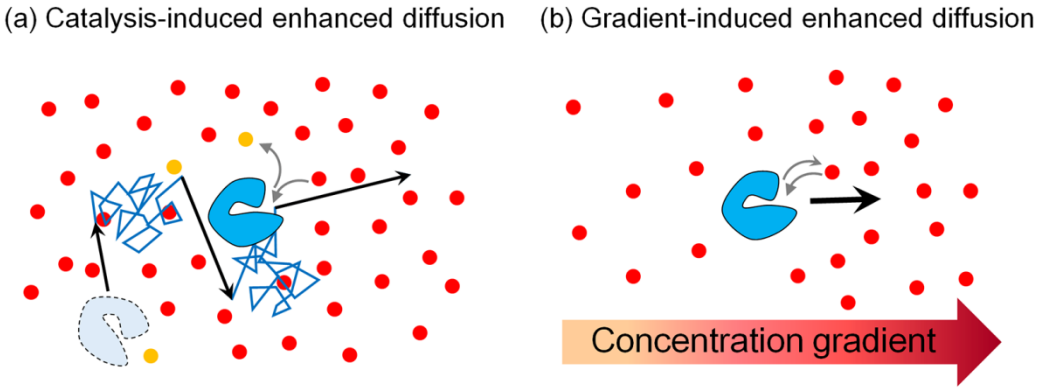

Fig. 3 | **Enhanced diffusion of a particle under catalytic and non-catalytic conditions. a** | Catalysis-induced enhanced diffusion was thought to originate from ballistic leaps driven by chemical reactions, independent of a concentration gradient of solutes. **b** | Enhanced diffusion occurs in the presence of a concentration gradient of substrates or products, relying on interactions between swimmers and solutes rather than any reactions directly.

Aside from FCS measurements, there are other independent methods to test the effect of enhanced diffusion. For example, DLS has been used to determine the diffusion coefficient of an aldolase in the presence and absence of its fructose-1,6-bisphosphate substrate,[74] a measurement that was also carried out using pulsed-field gradient nuclear magnetic resonance (PFG-NMR) spectroscopy.[75] Both experiments did not indicate any diffusion enhancement for aldolase. By using anti-Brownian electrokinetic (ABEL) trap-based single-molecule diffusometry, even alkaline phosphatase, a fast enzyme with a high typical turnover frequency of 10^4 s^{-1}, showed no diffusion enhancement during catalysis.[76] A comprehensive summary and discussion of the inconsistent experimental observations can be found in a recent critical review.[77]

A very recent investigation reiterated the claims regarding enhanced diffusion of seven enzymes that catalyzing exergonic reactions, including urease, phosphoglucoisomerase, acetylcholinesterase, hexokinase and others.[78] The magnitude of enhanced diffusion has a clear linear dependence on the Gibbs free energy release (ΔG) rate rather than the enthalpy change (ΔH), allowing for enhanced diffusion of enzyme such as aldolase, which mediates an endothermic ($\Delta H > 0$) but exergonic ($\Delta G < 0$) reaction. However, the detailed mechanism of how free energy changes drive enhanced diffusion remains unknown. We must not forget that

when the enzymatic reaction approaches equilibrium (ΔG = 0), the enzymes are still catalysing the forward and reverse reactions at equal rates. As Astumian has repeatedly pointed out,[79-81] individual enzymes have no awareness of the bulk reaction conditions, so for the enhanced diffusion to cease at equilibrium, the reverse reaction would have to precisely undo the movement of the forward reaction. The diffusive rotation between the reaction events makes this difficult to conceive.

The above contradictions implied the necessity to investigate the accuracy of fluorescence correlation measurements. A detailed experimental study described the potential sources of artefacts in FCS measurements of protein diffusion, revealing that the apparent diffusion of alkaline phosphatase originated from fluorescence quenching.[82] Another group found that the FCS artefacts were mainly from 4-nitrophenylphosphate-induced fluorescence quenching and blinking.[76] Dissociation of multimeric enzymes during catalysis has also been considered a possible origin of the observed enhanced diffusion of enzymes.[73,82] This hypothesis has been tested with urease, hexokinase, acetylcholinesterase and aldolase using four independent measurements: static light scattering, size-exclusion chromatography (SEC), DLS and FCS.[83] Each enzyme dissociates into its subunits at substrate concentration regimes exceeding the enzyme's Michaelis–Menten constant K_m. Although it is intuitive that substrate binding and the associated conformational changes can destabilize a multimeric enzyme complex, it is unclear why this would occur only when [substrate] > K_m. In comparison, molecular tracking with total internal reflection fluorescence (TIRF) microscopy showed the presence of multiple oligomeric states of urease as well as a threefold increase in its diffusion coefficient, although the authors concluded that the enhanced diffusion was not caused by enzyme dissociation.[84] This molecular tracking was conducted in a highly viscous solution (0.6% 88 kDa methylcellulose was added to slow diffusion and aid visualization) and it is unclear whether the conclusion can be generalized to common aqueous systems. Most importantly, the reliability of MSD analysis itself has recently been questioned,[85] which we will return to in a later section.

The present principles are not unique to enzymes. Nanoparticles that are tens of nanometres in diameter are subject to the same limits in sustaining the accelerated diffusion by chemical reactions unless the nanoparticles undergo diffusiophoresis or chemotaxis in a concentration gradient.[29]

[H2] Chemotaxis of enzymes and nanoparticles

Similar to microparticles, nanoparticles and macromolecules (especially enzymes) also exhibit migration in a solute or solvent concentration gradient. This is called chemotaxis when migration is toward regions of higher [solute] and antichemotaxis[62] when migration is toward lower [solute] (Fig. 3b). This phenomenon is generally observed in microfluidic devices and has been proposed as a principle for separation.[86] The mechanism responsible for this behaviour has been proposed to be diffusiophoresis arising from nonspecific interactions between particles and solutes[87] or specific active-site–substrate binding.[63,88] The chemotactic migration of enzymes, which is regulated by the local [substrate] and the substrate–enzyme binding constant, has been used to rationalize the formation of metabolons from glycolytic

enzymes — enzyme complexes in which the product of one enzyme is passed to the next enyzme.[63,89]

[H1] Diffusion of small molecules in chemical reactions

- The size of a small molecule is comparable to that of the surrounding solvent molecules, so any self-propelled motion of the molecule in question is rapidly randomized by the frequent collisions with solvent (D_r = 10^9–10^{12} s^{-1}).[90] In the absence of chemical reactions, the translational diffusion coefficient is given by the classic Einstein equation with a proper assessment of the effective radius of gyration of the diffusing entity in its environment.[91] The large ratio between drag and mass implies that any kinetic energy imparted on the swimmer during a reaction is quickly dissipated into heat through viscous friction, resulting in only a small displacement and negligible diffusion enhancement. For example, a 100 Da molecule with a 1 nm radius and 10 k_BT kinetic energy travels only 6 pm in H_2O before the kinetic energy has dissipated into the environment. Boosts of 10 k_BT kinetic energy repeating at a frequency of 10^4 s^{-1} would therefore increase the diffusion coefficient relative to the "unboosted" molecule only by a fraction of 10^{-9} . Only by implicitly and inexplicably assuming a solution viscosity as low as that of air can nm-scale displacements be generated.[21] For this reason, observations of enhanced diffusion of small molecules such as Grubb's 2nd generation catalyst should come as a surprise[17] because they cannot be explained by the changes in molecular radii during the reaction nor the presence of a chemical gradient. This was followed by an equally puzzling finding that both the passive tracer molecules and the catalyst exhibited enhanced diffusion in a reaction-velocity-dependent manner.[92] These observations raise the fundamental questions of how the enhanced diffusion is powered by the catalytic reaction and how the energy and momentum is transferred from the reactive species to the environment.[93] Molecular dynamics simulations suggested that chemical reactions could cause a significant enhancement in diffusion coefficients for Å-scale catalysts in an "argon-like solvent",[94] but the argon-like solvent has a viscosity which is more than thousand-fold lower than the viscosity of H_2O or organic solvents. Of course, an increase in viscosity increases energy dissipation, decreases the displacement per catalytic event and decreases the diffusion enhancement. More generally, the study of intramolecular vibrational energy redistribution (IVR) has shown that even if specific vibrational modes of a molecule are excited, the excitation spreads among the accessible vibrational modes on a femtosecond to picosecond timescale. This makes it difficult to channel the energy released from a reaction into a single degree of freedom, as would be necessary for propulsion.[95,96]

The diffusion coefficient measurements of Grubbs' 2nd generation catalyst, first measured using diffusion NMR, have since been replicated at higher temporal resolution.[97] The apparent diffusion coefficient increased in the first 25 min and then fell back to normal while the reaction rate decreased monotonically over time. No diffusion enhancement was found for reactions carried out in a narrow NMR tube. Collectively, these findings suggested that the observed enhanced diffusion of small molecules was caused by convection in the bulk solution.

The above discovery has not put an end to the debate regarding enhanced diffusion. Also using diffusion NMR, Wang et al. recently observed enhanced diffusion (by 2–20%) of reactants and catalysts and even solvents in common reactions including catalysed bimolecular reactions, azide–alkyne cycloaddition, ring-opening metathesis polymerization and Sonogashira coupling[18]. In contrast, no enhancement was observed for S_N1 and S_N2 nucleophilic substitution reactions (Fig. 4). Convection suppression pulses were applied to counteract reaction-induced convection. In parallel to the claims of enhanced enzyme diffusion during catalysis, it was claimed that the magnitude of diffusion enhancement was related to the free energy release rate. Shortly thereafter, another team showed that the apparent boost in mobility may originate from experimental artefacts caused by changes in signal intensities over time during the NMR measurements[98]. Such an effect could introduce systematic errors in the regression. When repeating the cycloaddition described by Wang et al., the team demonstrated that apparently faster or slower diffusion can be had simply by applying a monotonically increasing or decreasing magnetic field gradient. Wang et al. responded with experiments showing that the diffusion coefficients measured in randomized magnetic field gradients were identical to those measured in linearly changing gradients.[99] Furthermore, Wang et al. argued that the failure to reproduce the diffusion enhancement might be due to the different reaction rates.

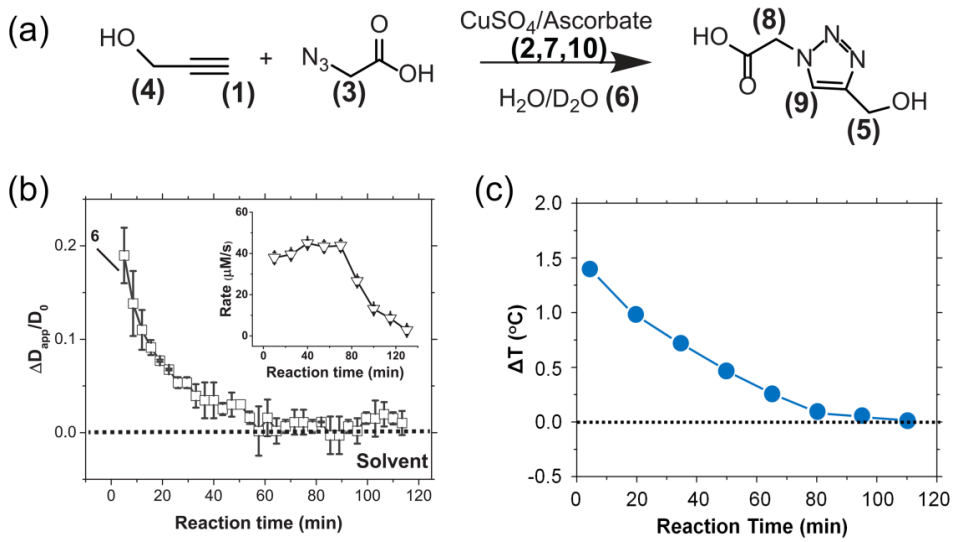

Fig. 4 | **A reported example of boosted molecular diffusion during an azide–alkyne cycloaddition. a** | The Cu-catalyzed reaction between propargyl alcohol and azidoacetic acid in H_2O/D_2O was monitored over time. **b** | The apparent enhancement in diffusion ΔD_{app}, normalized with respect to the diffusion coefficient D_0, of H_2O/D_2O solvent decreases over the course of the reaction. The respective reaction rates are pictured in the inset. **c** | The change in temperature during the reaction follows a similar trend. Parts **b** and **c** adapted with permission from Ref. 18, AAAS.

Independent of the argument whether boosted molecular diffusion is observable in diffusion NMR there appear to be other inconsistencies in Wang et al.'s paper. For the click reaction, the diffusion coefficient of the solvent gradually decreased to a normal value within 60

minutes while the reaction rate was constant over almost 80 minutes (Fig. 4b). This suggests that the reaction caused enhanced diffusion in the beginning of the reaction, but not towards the end. It is unclear why this should be the case. Curiously, the time course of the change in the diffusion coefficient was similar to the time course of the change in the temperature, which started 1.5 K above room temperature and dropped to room temperature within 60 min (Fig. 4c). Temperature changes can affect the observed diffusion coefficient because they greatly affect the viscosity of the aqueous solvent and can create convection artefacts. In ring-opening metathesis polymerization with the Grubbs 2nd generation catalyst, the diffusion of species over the course of the reaction must also be substantially affected by changes in composition and concentration of reactants that are present at high initial concentrations (hundreds of mM to 1 M). However, this factor has not been quantitatively accounted for when the observed changes in diffusion coefficients are assigned wholly to enhanced diffusion. We look forward to seeing more detailed discussion of this intriguing but controversial report.

[H1] Enhanced transport of passive tracers

Tracer particles are traditionally used to visualize the flow field in fluid dynamics. Ideally, the tracer particles are inert and provide high contrast to facilitate observation, while being small and of sufficiently low molar mass to follow the path of the surrounding fluid. In the study of microswimmers, tracers can be smaller, of similar size or substantially larger than the microswimmers themselves. The tracers move not only because they interact with the microswimmers but also because of their own Brownian motion and other flow fields such as convection.

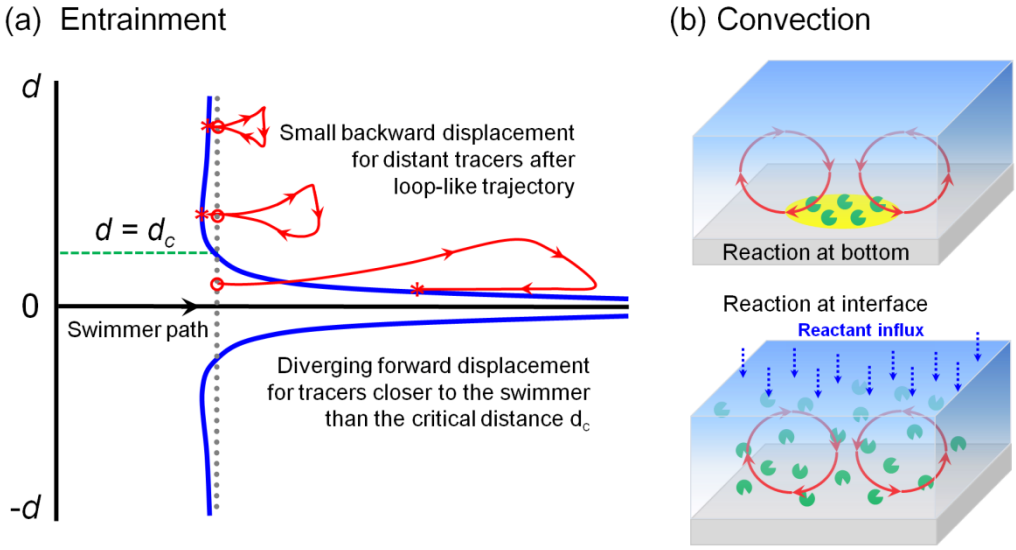

Fig. 5 | **Enhanced transport of tracers. a** | Typical trajectories of a sheet of tracer particles as a microswimmer moves from left to right. The initial positions of tracer particles are shown as a gray dotted line and the envelope of their final positions is shown in blue curves. Three trajectories of tracers (red curves) start from the open circles and end at the asterisks. The initial distance between the tracer and the swimmer path is denoted *d*. **b** | Tracer particles can be transported by convective flows induced by asymmetrically distributed reactions. These

flows can be established by, for example, surfaces decorated with immobilised enzymes or the introduction of reactants such as O_2 at the interface of a fluid layer. Part **a** adapted with permission from Ref. 100, Cambridge University Press.

[H2] Tracer transport due to flows produced by microswimmers

Microswimmers translate and rotate, exerting pressure and torque on surrounding fluid and establishing flow fields that could substantially affect the motion of passive tracer particles. The particles can be entrained forward if they are near the moving swimmer, and tend to move in closed loops if they are further from the swimmer (Fig. 5a).[100] The tracer trajectories are governed by factors that include the: geometry and size of the swimmer, swimming path length and velocity, distance between the swimmer and tracer, and boundary conditions. These can be further complicated by the Brownian motion of the tracer.[101] The increased mobility of tracers caused by active swimmers is of chemical and biological importance. For example, tracers in dilute suspensions of swimming bacteria exhibit enhanced diffusion.[102] Synthetic microswimmers have also shown an ability to agitate tracers. This enhanced diffusivity has been observed for 1–2 μm tracers in the presence of bimetallic Au–Pt rods (1.2 μm long × 0.4 μm diameter) swimming close to a surface through bipolar electrochemical propulsion.[103,104] The diffusion coefficient of the 2 μm tracer increased linearly from 0.15–0.3 $\mu m^2 s^{-1}$ as the swimmer density and velocity were increased. This observation fits well with a back-of-the-envelope calculation of the diffusion coefficient enhancement, which assumes that each tracer–swimmer encounter displaces the tracer by roughly the diameter of the swimmer. Tracer diffusion enhancement of 20–50% has also been measured in different enzymatic reactions for tracers ranging from the small molecule rhodamine B to 50 nm and 100 nm polystyrene particles, lending support to enzyme propulsion.[105] Puzzlingly, the tracer diffusion enhancement was the same for the fast enzyme urease and the $10^3\times$ slower enzyme aldolase at the same enzyme concentration. This seems counterintuitive because the swimmer activity determines the frequency of encounters between swimmers and tracers, and thereby the tracer diffusion enhancement. Tracer motion in the presence of bubble-propelled micromotors was further amplified by the gravity-driven motion of the generated bubbles.[106]

[H2] Reaction-induced convection

The concentration gradients produced by chemical reactions can give rise to convective flows that pump tracer particles (Fig. 5b). For example, surface-immobilised enzymes such as glucose oxidase, urease, lipase, catalase and DNA polymerase can pump fluids and particles in the presence of their substrates through convective flow.[107,108] The resulting flow velocity is on the order of $\mu m s^{-1}$ and often increases with increasing reaction rates. Similarly, enzymatic reactions at the air–liquid interface of a homogenous solution can also drive Rayleigh–Bénard-type convection if the reaction increases the solutal density, leading to flow velocities of up to 1 $mm s^{-1}$.[109] Because Rayleigh–Bénard-type convection occurs only above a critical barrier governed by the Rayleigh number (proportional to the cube of solution depth), the solution must typically be at least 1 mm deep. The contribution of thermal buoyancy in such systems is usually negligible[110] but the gradient in surface tension may play a more important role especially when the system dimensions become smaller.[111] The requirements for reaction-induced convection are frequently met in experiments aimed at

finding enhanced diffusion, and convection has to be carefully ruled out as a mechanism responsible for the observations.

[H1] Reliability of diffusion coefficient measurements

Many papers report diffusion enhancements as small as 20%, such that the accuracy and precision of measurements is crucial. MSD analysis has been widely used as a standard measurement to determine diffusion coefficients of micro-/nanoswimmers[23,112] and even single enzymes.[84] A recent test on the reproducibility of MSD analysis has alerted the community to possible misinterpretations.[85] The test was conducted by tracing size-standard 100 nm spherical colloidal particles using a Nanosight NS300 (Malvern) instrument. Based on 244 particle tracks, the analysis afforded a precise and accurate diffusion coefficient, with errors smaller than 1%. However, using a subset of only 24 tracks can lead results with 30% deviations. Although the errors should be non-directional, biased selection further widened the uncertainty from –55.5% to +68.0%. The experimental uncertainty also comes from the 2D projection of the 3D Brownian paths but can be lowered by increasing the size of the dataset. The strikingly large inaccuracy indicated that MSD analysis with less than 50 tracks is unreliable for claiming a diffusion enhancement of 20% or less. Unfortunately, few investigations in the past decade used the desired sample size, rendering the measured enhancements potentially not statistically significant. A critical examination of the experimental error estimates is important when using these enhancements to claim statistical significance of observed enhanced diffusion. For example, estimates of experimental errors are likely too small if statistically significant variations in the diffusion enhancement are observed at different saturating substrate concentrations.[84]

FCS can be applied to measure absolute diffusion coefficients of molecular and nanoscale swimmers by analyzing fluctuations in emission from a few molecules freely diffusing in and out of the observation volume.[113] The standard deviation of autocorrelation functions has been studied analytically and experimentally[114-116] but the highly nonlinear relationship between the diffusion coefficient and the autocorrelation function makes it hard to estimate the errors. A statistical analysis of diffusion coefficients extracted from FCS measurements suggested that their accuracy was sensitive to a molecule's brightness and concentration, as well as the measurement time.[117] To achieve a given accuracy, experimental conditions have to be carefully optimized otherwise FCS can be extremely error-prone. A satisfactory accuracy for the diffusion coefficient from FCS measurements is 10%[118] and according to an IUPAC technical report, dual-focus FCS, a more accurate modification of FCS, can further improve the accuracy to 4%.[119] However, FCS measurements are prone to artefacts caused by protein dissociation and aggregation, concentration changes due to surface adsorption, fluorophore quenching and the presence of freely-diffusing dyes, often resulting in enhanced diffusion coefficients.[82] Granick and colleagues defended the robustness of FCS, arguing that the influence of quenching is manageable if the timescales of diffusion can be well separated from the timescales of photophysical processes.[120] However, their experiments on dye-labeled bovine serum albumin in the presence still showed changes in the measured diffusion coefficient of ~15% and >50% in the presence of 0.5 mM and 1 mM tryptophan (a fluorescence quencher), respectively, even though albumin does not catalyze any reactions.[120]

In principle, stimulated emission depletion (STED) FCS facilitates diffusion measurements but in practice the method introduces new complexities, such as sensitivity to optical aberrations and potential interactions between the diffusing molecule and the powerful infrared laser.[121,122]

In addition to the above methods targeting one or a few objects, DLS can assess the ensemble diffusivity of objects with sizes from several nanometres to micrometres. Most commercial DLS instruments are claimed to have a measurement accuracy of 2% according to the International Standard ISO13321. Of course, this specification is achievable when using standard samples under optimized conditions. However, the R^6 dependence of scattering intensity makes the measurement extremely sensitive to particle aggregation and the presence of adventitious larger particles like dust. Especially for proteins several nanometres in diameter, the weak scattering signal, the ease of aggregation, and the structural and thermal instability easily lower the accuracy. In practice, the uncalibrated viscosity of solutions containing different concentrations of reagents can also cause systematic inaccuracies of up to 5%. Variations in concentration, labware cleanliness and temperature will result in additional random uncertainties. It is common to expect an experimental error of at least 10% for protein samples unless special care has been taken during the measurement.

Diffusion NMR is a powerful technique to determine translational diffusion coefficients of molecules and can resolve different compounds with different diffusivities in a mixture according to their characteristic chemical shifts. The measurement makes use of NMR signal attenuation, which depends on both molecular diffusion and the applied magnetic field gradient pulses.[123] Although an accuracy of 2% is possible, achieving this demands high-quality data without spectral overlap and ideal experimental conditions.[124] Systematic artefacts mainly come from inherent non-uniformity of the field gradient based on the gradient coil design, convection triggered by temperature gradients, and eddy currents caused by sudden gradient switching.[124,125] To achieve high-quality diffusion data, the gradient non-uniformity needs to be compensated for by pulse calibration,[126] the convection needs to be avoided with a convection-compensated pulse sequence[123] and the eddy currents need to be reduced by using a shielded gradient system and/or a smoothly changing pulse.[124] If the experiments are not carefully carried out under optimized conditions, the measured diffusion coefficient can appear larger.

Overall, there exists a variety of common techniques to measure diffusion, all of which have their associated errors. Given the typical accuracy and precision of these techniques, reported diffusion enhancements within 20% are on the edge of being statistically significant, especially for enzymes and synthetic swimmers at the nanoscale.

[H1] Applications and efficiencies of nano- and microswimmers

The accelerated diffusion or locomotion of nano- and microswimmers, tracers and solvents has inspired applications in bioseparation, environmental remediation, detection, drug delivery and precision surgery, among others. Taking advantage of the enhanced diffusion of enzymes in their corresponding substrate concentration gradient, chemotactic separation of

active enzymes (catalase and urease) from the inactive ones has been demonstrated in a microfluidic device,[127] while anti-chemotactic migration of urease has also been proposed.[62] In addition, active swimmers can agitate the surrounding fluid, sense environmental changes, navigate living tissues and penetrate cell membranes.[128] In light of these properties, a series of creative and intriguing demonstrations has shown a broad range of applications including the detection and decontamination of nerve agents,[7,129] acid neutralization in vivo,[130] biodetoxification of pathogenic bacteria and toxins[131] and intracellular delivery of siRNA or drugs[8,132,133]. For example, self-propelled polymer–Pt composite micromotors can accelerate the oxidative detoxification of organophosphorus compounds,[7] and enzyme-powered chemotactic polymersomes can cross the blood–brain barrier, an important property in neuromedicine.[133] These and other efforts have been discussed in detail in recent reviews.[134-140]

Although the ability of some synthetic swimmers to harvest energy from their surroundings greatly broadens their possible applications, their energy conversion efficiency (the quotient of mechanical energy produced to chemical energy consumed) is far below that of biological counterparts (Fig. 6). For example, the motor protein kinesin catalyzes exothermic ATP hydrolysis as it walks along a microtubule and can do mechanical work on an external load in excess of 50% of the chemical energy consumed.[141] More strikingly, the free energy transduction efficiency of the rotary motor F_1-ATPase has been reported to be nearly 100%,[142] although the irreversible heat dissipation by torque-induced mechanical slip would lower it to 40−80%.[143] The bacterium *Escherichia coli*, a microscale natural swimmer that propels itself with rotating flagellar filaments, has an efficiency of 2%.[144] In comparison, synthetic swimmers are several orders of magnitude less efficient. For example, the energy conversion efficiency of Au–Pt nanorods (2 μm in length and 370 nm in diameter and swimming at a speed of 10 μms^{-1}) propelled by the decomposition of H_2O_2 has been estimated to be 10^{-9},[39] and the typical efficiency of self-electrophoretic bimetallic particles is on the order of 10^{-8}–10^{-9}.[145] After optimizing morphology and catalytic activity, the highest efficiency observed for a diffusiophoretic motor is 10^{-5} for a Ag-based Janus spherical particle.[146] Microswimmers propelled by bubble generation have so far exhibited an even lower efficiency of ~10^{-10}. It is possible to prepare helical nanobelts that mimic bacterial flagella and obtain an efficiency of 10^{-2}–10^{-3}, but the mimics are powered by an external rotating magnetic field rather than being self-propelled.[39,147]

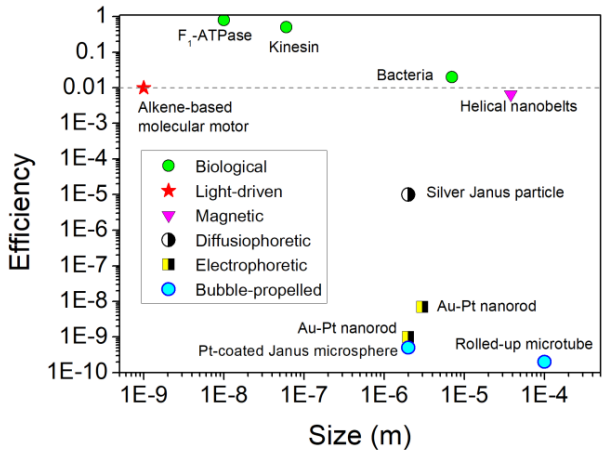

Fig. 6 | **The efficiencies of typical microscopic motors.** Kinesin[141], F_1-ATPase[143], *E. coli*[144], alkene-based molecular motors[148], helical nanobelts[147], Ag Janus particles[146], Au–Pt nanorods[39,145], Pt-coated Janus particles[52] and rolled-up microtubes[149] have diverse propulsion mechanisms. Their efficiencies, several estimates of which were obtained from Ref. 145, span several orders of magnitude. The alkene-based molecular motor is driven by light irradiation and helical nanobelts are powered by external magnetic fields instead of chemical reactions.

The extremely low efficiency of synthetic nano- and microswimmers (or motors) severely limits their application[150] because performing even small amounts of work requires enormous amounts of chemical fuel (for example, 1 M H_2O_2). This can cause toxicity and insolubility, but also leads to ambiguity — is the observed effect due to work or the vastly larger heat generated as a byproduct by the motor? One of the mechanistic origins is a mismatch between the large forces that can be generated during the cleavage and formation of bonds and the small resistance offered by the fluid environment. Motor proteins are only efficient if they have a loaded cytoskeletal filament to pull against, and similarly the flagellar motor needs the flagellum as a transducer. In the examples discussed above, the catalytic particles 'swim' when they need to 'row' — they push locally against small loads whereas a gearing mechanism such as an oar would enable a flow field with smaller velocity gradients (implying smaller frictional losses) and a better matching of force generation and load. Improving the efficiency will be crucial for developing the next generation of synthetic motors that can work in physiological environments with reasonable concentrations of potential fuels (such as glucose, O_2 and H^+). To realize a high-performance propulsion system, we require an efficient chemical–mechanical coupling mechanism as prime mover, a suitable power transmission system and a well-designed actuator to work in concert.

[H1] Summary

Chemically powered molecular and nano-/microswimmers that exhibit enhanced diffusion or swimming relative to the expected Brownian diffusion are attractive because they can convert chemical energy to potentially useful mechanical work. Molecular, nanoscale and microscale systems exhibiting diffusion enhancement have been intensively studied and hotly debated in the past decade. The debates have mainly focused on the underlying propulsion mechanisms and the size of the effect which may vary from case-to-case as the swimmers differ in size and

architectures. In this Perspective, we have systematically categorized reported observations of enhanced diffusion according to the sizes of the swimmers. Microscale (or larger) swimmers can exhibit ballistic motion while nanoscale or molecular scale swimmers exhibit 'active' diffusion with the observed diffusion enhancement typically being near the limits of experimental reproducibility and statistical significance. Rigorous analysis is thus desired to clarify the reliability, origin and achievable magnitude of diffusion enhancement.

The study of active diffusion on molecular, nano- and microscales opens an avenue to the design of synthetic machines that perform work in the presence of comparatively large thermal fluctuations. The implementation of these microscopic machines would enable us to steer chemical reactions and biological processes, and would consequently lead to revolutionary developments in diverse areas including but not limited to reaction regulation, cell manipulation and precision medicine. Although evolution has provided sophisticated examples such as motor proteins and transcriptional machineries, the construction of synthetic microscopic machines is challenging. The previously reported synthetic swimmers with enhanced diffusivity, regardless of their validation, are still much simpler and less efficient compared to their biological counterparts. Future efforts should focus on understanding chemo-mechanical coupling and the structure–function relationship of these microscopic machines, so that we can gain fundamental insights for the construction of more sophisticated machines that may perform complex tasks beyond speeding up diffusion and mixing. For example, the latest advance in this field is a computational design of millimetre-size gears driven by enzymatic reaction-induced convections,[151] putting us a step closer to constructing chemically-powered functional machines. We expect to see breakthroughs such as de novo designed protein motors and bio-inorganic hybrid components and machines that can directly convert chemical energy into mechanical work. These efforts will greatly expand our toolbox on the molecular, subcellular and even macroscopic scales.

[H1] References

1 Lancia, F., Ryabchun, A. & Katsonis, N. Life-like motion driven by artificial molecular machines. *Nat. Rev. Chem.* **3**, 536–551 (2019).

2 Aprahamian, I. The future of molecular machines. *ACS Cent. Sci.* **6**, 347–358 (2020).

3 Wang, J. Can man-made nanomachines compete with nature biomotors? *ACS Nano* **3**, 4–9 (2009).

4 Ozin, G. A., Manners, I., Fournier-Bidoz, S. & Arsenault, A. Dream nanomachines. *Adv. Mater.* **17**, 3011–3018 (2005).

5 Carter, N. J. & Cross, R. A. Mechanics of the kinesin step. *Nature* **435**, 308–312 (2005).

6 García-López, V. *et al.* Molecular machines open cell membranes. *Nature* **548**, 567–572 (2017).

7 Orozco, J. *et al.* Micromotor-based high-yielding fast oxidative detoxification of chemical threats. *Angew. Chem. Int. Ed.* **52**, 13276–13279 (2013).

8 de Ávila, B. E.-F. *et al.* Micromotor-enabled active drug delivery for in vivo treatment of stomach infection. *Nat. Commun.* **8**, 272 (2017).

9 Saper, G. & Hess, H. Synthetic systems powered by biological molecular motors.

Chem. Rev. **120**, 288–309 (2020).

10 Roke, D., Wezenberg, S. J. & Feringa, B. L. Molecular rotary motors: unidirectional motion around double bonds. *Proc. Natl Acad. Sci. USA* **115**, 9423–9431 (2018).

11 Zhang, L., Marcos, V. & Leigh, D. A. Molecular machines with bio-inspired mechanisms. *Proc. Natl Acad. Sci. USA* **115**, 9397–9404 (2018).

12 Noji, H., Yasuda, R., Yoshida, M. & Kinosita, K. Direct observation of the rotation of F_1-ATPase. *Nature* **386**, 299–302 (1997).

13 Soong, R. K. *et al.* Powering an inorganic nanodevice with a biomolecular motor. *Science* **290**, 1555–1558 (2000).

14 Dennis, J. R., Howard, J. & Vogel, V. Molecular shuttles: directed motion of microtubules along nanoscale kinesin tracks. *Nanotechnology* **10**, 232 (1999).

15 Hess, H. Toward devices powered by biomolecular motors. *Science* **312**, 860–861 (2006).

16 Magdanz, V. *et al.* Spermatozoa as functional components of robotic microswimmers. *Adv. Mater.* **29**, 1606301 (2017).

17 Pavlick, R. A., Dey, K. K., Sirjoosingh, A., Benesi, A. & Sen, A. A catalytically driven organometallic molecular motor. *Nanoscale* **5**, 1301–1304 (2013).

18 Wang, H. *et al.* Boosted molecular mobility during common chemical reactions. *Science* **369**, 537–541 (2020).

19 Muddana, H. S., Sengupta, S., Mallouk, T. E., Sen, A. & Butler, P. J. Substrate catalysis enhances single-enzyme diffusion. *J. Am. Chem. Soc.* **132**, 2110–2111 (2010).

20 Sengupta, S. *et al.* Enzyme molecules as nanomotors. *J. Am. Chem. Soc.* **135**, 1406–1414 (2013).

21 Riedel, C. *et al.* The heat released during catalytic turnover enhances the diffusion of an enzyme. *Nature* **517**, 227–230 (2015).

22 Ma, X., Hortelão, A. C., Patiño, T. & Sánchez, S. Enzyme catalysis to power micro/nanomachines. *ACS Nano* **10**, 9111–9122 (2016).

23 Ma, X. *et al.* Enzyme-powered hollow mesoporous Janus nanomotors. *Nano Lett.* **15**, 7043–7050 (2015).

24 Purcell, E. M. Life at low Reynolds number. *Am. J. Phys.* **45**, 3–11 (1977).

25 Ishimoto, K. & Yamada, M. A rigorous proof of the scallop theorem and a finite mass effect of a microswimmer. arXiv:1107.5938 (2011).

26 Lauga, E. Enhanced diffusion by reciprocal swimming. *Phys. Rev. Lett.* **106**, 178101 (2011).

27 Howse, J. R. *et al.* Self-motile colloidal particles: from directed propulsion to random walk. *Phys. Rev. Lett.* **99**, 048102 (2007).

28 Yamamoto, D. & Shioi, A. Self-propelled nano/micromotors with a chemical reaction: underlying physics and strategies of motion control. *KONA Powder Part. J.* **32**, 2–22 (2015).

29 Lee, T. C. *et al.* Self-propelling nanomotors in the presence of strong Brownian forces. *Nano Lett.* **14**, 2407–2412 (2014).

30 Dey, K. K. *et al.* Micromotors powered by enzyme catalysis. *Nano Lett.* **15**, 8311–8315 (2015).

31 Pavel, I.-A., Bunea, A.-I., David, S. & Gáspár, S. Nanorods with biocatalytically induced self-electrophoresis. *ChemCatChem* **6**, 866–872 (2014).

32 Wilson, D. A., Nolte, R. J. M. & van Hest, J. C. M. Autonomous movement of platinum-loaded stomatocytes. *Nat. Chem.* **4**, 268–274 (2012).

33 Paxton, W. F. *et al.* Catalytic nanomotors: autonomous movement of striped nanorods. *J. Am. Chem. Soc.* **126**, 13424–13431 (2004).

34 Abdelmohsen, L. K. E. A. *et al.* Dynamic loading and unloading of proteins in polymeric stomatocytes: formation of an enzyme-loaded supramolecular nanomotor. *ACS Nano* **10**, 2652–2660 (2016).

35 Ma, X., Wang, X., Hahn, K. & Sánchez, S. Motion control of urea-powered biocompatible hollow microcapsules. *ACS Nano* **10**, 3597–3605 (2016).

36 Kim, D., Liu, A., Diller, E. & Sitti, M. Chemotactic steering of bacteria propelled microbeads. *Biomed. Microdevices* **14**, 1009–1017 (2012).

37 Sattayasamitsathit, S., Kaufmann, K., Galarnyk, M., Vazquez-Duhalt, R. & Wang, J. Dual-enzyme natural motors incorporating decontamination and propulsion capabilities. *RSC Adv.* **4**, 27565–27570 (2014).

38 Mano, N. & Heller, A. Bioelectrochemical propulsion. *J. Am. Chem. Soc.* **127**, 11574–11575 (2005).

39 Paxton, W. F., Sen, A. & Mallouk, T. E. Motility of catalytic nanoparticles through self-generated forces. *Chem. Eur. J.* **11**, 6462–6470 (2005).

40 Wang, W., Duan, W., Sen, A. & Mallouk, T. E. Catalytically powered dynamic assembly of rod-shaped nanomotors and passive tracer particles. *Proc. Natl Acad. Sci. USA* **110**, 17744–17749 (2013).

41 Bunea, A.-I., Pavel, I.-A., David, S. & Gáspár, S. Modification with hemeproteins increases the diffusive movement of nanorods in dilute hydrogen peroxide solutions. *Chem. Commun.* **49**, 8803–8805 (2013).

42 Jun, I.-K. & Hess, H. A biomimetic, self-pumping membrane. *Adv. Mater.* **22**, 4823–4825 (2010).

43 Abécassis, B., Cottin-Bizonne, C., Ybert, C., Ajdari, A. & Bocquet, L. Boosting migration of large particles by solute contrasts. *Nat. Mater.* **7**, 785–789 (2008).

44 Paustian, J. S. *et al.* Direct measurements of colloidal solvophoresis under imposed solvent and solute gradients. *Langmuir* **31**, 4402–4410 (2015).

45 Velegol, D., Garg, A., Guha, R., Kar, A. & Kumar, M. Origins of concentration gradients for diffusiophoresis. *Soft Matter* **12**, 4686–4703 (2016).

46 Golestanian, R., Liverpool, T. B. & Ajdari, A. Propulsion of a molecular machine by asymmetric distribution of reaction products. *Phys. Rev. Lett.* **94**, 220801 (2005).

47 Arqué, X. et al. Intrinsic enzymatic properties modulate the self-propulsion of micromotors. *Nat. Commun.* **10**, 2826 (2019).

48 Patiño, T. *et al.* Influence of enzyme quantity and distribution on the self-propulsion of non-Janus urease-powered micromotors. *J. Am. Chem. Soc.* **140**, 7896–7903 (2018).

49 Ismagilov, R. F., Schwartz, A., Bowden, N. & Whitesides, G. M. Autonomous movement and self-assembly. *Angew. Chem. Int. Ed.* **41**, 652–654 (2002).

50 Fournier-Bidoz, S., Arsenault, A. C., Manners, I. & Ozin, G. A. Synthetic

self-propelled nanorotors. *Chem. Commun.* **4**, 441–443 (2005).

51 Sitt, A. *et al.* Microscale rockets and picoliter containers engineered from electrospun polymeric microtubes. *Small* **12**, 1432–1439 (2016).

52 Gibbs, J. G. & Zhao, Y.-P. Autonomously motile catalytic nanomotors by bubble propulsion. *Appl. Phys. Lett.* **94**, 163104 (2009).

53 Nourhani, A., Karshalev, E., Soto, F. & Wang, J. Multigear bubble propulsion of transient micromotors. *Research* **2020**, 7823615 (2020).

54 Wang, H., Zhao, G. & Pumera, M. Beyond platinum: bubble-propelled micromotors based on Ag and MnO_2 catalysts. *J. Am. Chem. Soc.* **136**, 2719–2722 (2014).

55 Gao, W., Pei, A. & Wang, J. Water-driven micromotors. *ACS Nano* **6**, 8432–8438 (2012).

56 Zhang, X., Chen, C., Wu, J. & Ju, H. Bubble-propelled jellyfish-like micromotors for DNA sensing. *ACS Appl. Mater. Interfaces* **11**, 13581–13588 (2019).

57 Nijemeisland, M., Abdelmohsen, L. K. E. A., Huck, W. T. S., Wilson, D. A. & van Hest, J. C. M. A compartmentalized out-of-equilibrium enzymatic reaction network for sustained autonomous movement. *ACS Cent. Sci.* **2**, 843–849 (2016).

58 Gao, W. *et al.* Artificial micromotors in the mouse's stomach: a step toward in vivo use of synthetic motors. *ACS Nano* **9**, 117–123 (2015).

59 Li, J. *et al.* Enteric micromotor can selectively position and spontaneously propel in the gastrointestinal tract. *ACS Nano* **10**, 9536–9542 (2016).

60 Wang, T., Zheng, M., Wang, L., Ji, L. & Wang, S. Crucial role of an aerophobic substrate in bubble-propelled nanomotor aggregation. *Nanotechnology* **31**, 355504 (2020).

61 Chi, Q., Wang, Z., Tian, F., You, J. & Xu, S. A review of fast bubble-driven micromotors powered by biocompatible fuel: low-concentration fuel, bioactive fluid and enzyme. *Micromachines* **9**, 537 (2018).

62 Jee, A.-Y., Dutta, S., Cho, Y.-K., Tlusty, T. & Granick, S. Enzyme leaps fuel antichemotaxis. *Proc. Natl Acad. Sci. USA* **115**, 14–18 (2018).

63 Zhao, X. *et al.* Substrate-driven chemotactic assembly in an enzyme cascade. *Nat. Chem.* **10**, 311–317 (2018).

64 Illien, P. *et al.* Exothermicity is not a necessary condition for enhanced diffusion of enzymes. *Nano Lett.* **17**, 4415–4420 (2017).

65 Golestanian, R. Synthetic mechanochemical molecular swimmer. *Phys. Rev. Lett.* **105**, 018103 (2010).

66 Golestanian, R. Enhanced diffusion of enzymes that catalyze exothermic reactions. *Phys. Rev. Lett.* **115**, 108102 (2015).

67 Tsekouras, K., R. C., Gabizon, R., Marqusee, S., Pressé, S., Bustamante, C. Comment on "enhanced diffusion of enzymes that catalyze exothermic reactions" by Golestanian, R. *arXiv:1608.05433* (2016).

68 Golestanian, R. Reply to comment on "enhanced diffusion of enzymes that catalyze exothermic reactions". *arXiv:1608.07469* (2016).

69 Illien, P., Adeleke-Larodo, T. & Golestanian, R. Diffusion of an enzyme: the role of fluctuation-induced hydrodynamic coupling. *EPL* **119**, 40002 (2017).

70 Adeleke-Larodo, T., Illien, P. & Golestanian, R. Fluctuation-induced hydrodynamic

coupling in an asymmetric, anisotropic dumbbell. *Eur. Phys. J. E* **42**, 1–10 (2019).
71 Bai, X. & Wolynes, P. G. On the hydrodynamics of swimming enzymes. *J. Chem. Phys.* **143**, 165101 (2015).
72 Feng, M. & Gilson, M. K. A thermodynamic limit on the role of self-propulsion in enhanced enzyme diffusion. *Biophys. J.* **116**, 1898–1906 (2019).
73 Zhang, Y. & Hess, H. Enhanced diffusion of catalytically active enzymes. *ACS Cent. Sci.* **5**, 939–948 (2019).
74 Zhang, Y., Armstrong, M. J., Bassir Kazeruni, N. M. & Hess, H. Aldolase does not show enhanced diffusion in dynamic light scattering experiments. *Nano Lett.* **18**, 8025–8029 (2018).
75 Günther, J.-P., Majer, G. & Fischer, P. Absolute diffusion measurements of active enzyme solutions by NMR. *J. Chem. Phys.* **150**, 124201 (2019).
76 Chen, Z. *et al.* Single-molecule diffusometry reveals no catalysis-induced diffusion enhancement of alkaline phosphatase as proposed by FCS experiments. *Proc. Natl Acad. Sci. USA* **117**, 21328–21335 (2020).
77 Feng, M. & Gilson, M. K. Enhanced diffusion and chemotaxis of enzymes. *Annu. Rev. Biophys.* **49**, 87–105 (2020).
78 Jee, A.-Y., Tsvi, T. & Granick, S. Master curve of boosted diffusion for 10 catalytic enzymes. *Proc. Natl Acad. Sci. USA* **117**, 29435–29441 (2020).
79 Astumian, R. D. Microscopic reversibility as the organizing principle of molecular machines. *Nat. Nanotechnol.* **7**, 684–688 (2012).
80 Astumian, R. D. Thermodynamics and kinetics of molecular motors. *Biophys. J.* **98**, 2401–2409 (2010).
81 Astumian, R. D. Trajectory and cycle-based thermodynamics and kinetics of molecular machines: the importance of microscopic reversibility. *Acc. Chem. Res.* **51**, 2653–2661 (2018).
82 Günther, J.-P., Börsch, M. & Fischer, P. Diffusion measurements of swimming enzymes with fluorescence correlation spectroscopy. *Acc. Chem. Res.* **51**, 1911–1920 (2018).
83 Jee, A.-Y., Chen, K., Tlusty, T., Zhao, J. & Granick, S. Enhanced diffusion and oligomeric enzyme dissociation. *J. Am. Chem. Soc.* **141**, 20062–20068 (2019).
84 Xu, M., Ross, J. L., Valdez, L. & Sen, A. Direct single molecule imaging of enhanced enzyme diffusion. *Phys. Rev. Lett.* **123**, 128101 (2019).
85 Novotný, F. & Pumera, M. Nanomotor tracking experiments at the edge of reproducibility. *Sci. Rep.* **9**, 13222 (2019).
86 Seo, M., Park, S., Lee, D., Lee, H. & Kim, S. J. Continuous and spontaneous nanoparticle separation by diffusiophoresis. *Lab Chip* **20**, 4118–4127 (2020).
87 Schurr, J. M., Fujimoto, B. S., Huynh, L. & Chiu, D. T. A theory of macromolecular chemotaxis. *J. Phys. Chem. B* **117**, 7626–7652 (2013).
88 Agudo-Canalejo, J., Illien, P. & Golestanian, R. Phoresis and enhanced diffusion compete in enzyme chemotaxis. *Nano Lett.* 18, 2711–2717 (2018).
89 Mohajerani, F., Zhao, X., Somasundar, A., Velegol, D. & Sen, A. A theory of enzyme chemotaxis: from experiments to modeling. *Biochemistry* **57**, 6256–6263 (2018).
90 Huang, R. *et al.* Direct observation of the full transition from ballistic to diffusive

Brownian motion in a liquid. *Nat. Phys.* **7**, 576–580 (2011).
91 Rossi, C. & Bianchi, E. Diffusion of small molecules. *Nature* **189**, 822–824 (1961).
92 Dey, K. K. *et al.* Dynamic coupling at the Ångström scale. *Angew. Chem. Int. Ed.* **55**, 1113–1117 (2016).
93 Dey, K. K. Dynamic coupling at low Reynolds number. *Angew. Chem. Int. Ed.* **58**, 2208–2228 (2019).
94 Colberg, P. H. & Kapral, R. Ångström-scale chemically powered motors. *EPL* **106**, 30004 (2014).
95 Gruebele, M. & Wolynes, P. G. Vibrational energy flow and chemical reactions. *Acc. Chem. Res.* **37**, 261–267 (2004).
96 Hess, H., Asmis, K. R., Leisner, T. & Wöste, L. Vibrational wave packet dynamics in the silver tetramer probed by NeNePo femtosecond pump–probe spectroscopy. *Eur. Phys. J. D* **16**, 145–149 (2001).
97 MacDonald, T. S. C., Price, W. S., Astumian, R. D. & Beves, J. E. Enhanced diffusion of molecular catalysts is due to convection. *Angew. Chem. Int. Ed.* **58**, 18864–18867 (2019).
98 Günther, J.-P. *et al.* Comment on "boosted molecular mobility during common chemical reactions". *Science* **371**, eabe8322 (2021).
99 Wang, H. *et al.* Response to comment on "boosted molecular mobility during common chemical reactions". *Science* **371**, eabe8678 (2021).
100 Pushkin, D. O., Shum, H. & Yeomans, J. M. Fluid transport by individual microswimmers. *J. Fluid Mech.* **726**, 5–25 (2013).
101 Mathijssen, A. J. T. M., Pushkin, D. O. & Yeomans, J. M. Tracer trajectories and displacement due to a micro-swimmer near a surface. *J. Fluid Mech.* **773**, 498–519 (2015).
102 Morozov, A. & Marenduzzo, D. Enhanced diffusion of tracer particles in dilute bacterial suspensions. *Soft Matter* **10**, 2748–2758 (2014).
103 Miño, G. *et al.* Enhanced diffusion due to active swimmers at a solid surface. *Phys. Rev. Lett.* **106**, 048102 (2011).
104 Wang, Y. *et al.* Bipolar electrochemical mechanism for the propulsion of catalytic nanomotors in hydrogen peroxide solutions. *Langmuir* **22**, 10451–10456 (2006).
105 Zhao, X. *et al.* Enhanced diffusion of passive tracers in active enzyme solutions. *Nano Lett.* **17**, 4807–4812 (2017).
106 Orozco, J. *et al.* Bubble-propelled micromotors for enhanced transport of passive tracers. *Langmuir* **30**, 5082–5087 (2014).
107 Sengupta, S. *et al.* Self-powered enzyme micropumps. *Nat. Chem.* **6**, 415–422 (2014).
108 Sengupta, S. *et al.* DNA polymerase as a molecular motor and pump. *ACS Nano* **8**, 2410–2418 (2014).
109 Zhang, Y., Tsitkov, S. & Hess, H. Complex dynamics in a two-enzyme reaction network with substrate competition. *Nat. Catal.* **1**, 276–281 (2018).
110 Ortiz-Rivera, I., Shum, H., Agrawal, A., Sen, A. & Balazs, A. C. Convective flow reversal in self-powered enzyme micropumps. *Proc. Natl Acad. Sci. USA* **113**, 2585–2590 (2016).
111 Maroto, J. A., Pérez-Muñuzuri, V. & Romero-Cano, M. S. Introductory analysis of

Benard–Marangoni convection. *Eur. J. Phys.* **28**, 311–320 (2007).

112 Cheang, U. K., Roy, D., Lee, J. H. & Kim, M. J. Fabrication and magnetic control of bacteria-inspired robotic microswimmers. *Appl. Phys. Lett.* **97**, 213704 (2010).

113 Elson, E. L. Fluorescence correlation spectroscopy: past, present, future. *Biophys. J.* **101**, 2855–2870 (2011).

114 Koppel, D. E. Statistical accuracy in fluorescence correlation spectroscopy. *Phys. Rev. A* **10**, 1938–1945 (1974).

115 Wohland, T., Rigler, R. & Vogel, H. The standard deviation in fluorescence correlation spectroscopy. *Biophys. J.* **80**, 2987–2999 (2001).

116 Saffarian, S. & Elson, E. L. Statistical analysis of fluorescence correlation spectroscopy: the standard deviation and bias. *Biophys. J.* **84**, 2030–2042 (2003).

117 Enderlein, J., Gregor, I., Patra, D. & Fitter, J. Statistical analysis of diffusion coefficient determination by fluorescence correlation spectroscopy. *J. Fluoresc.* **15**, 415–422 (2005).

118 Heinemann, F., Betaneli, V., Thomas, F. A. & Schwille, P. Quantifying lipid diffusion by fluorescence correlation spectroscopy: a critical treatise. *Langmuir* **28**, 13395–13404 (2012).

119 Enderlein, J. Fluorescence correlation spectroscopy (IUPAC Technical Report). *Pure Appl. Chem.* **85**, 999–1016 (2013).

120 Kandula, H. N., Jee, A.-Y. & Granick, S. Robustness of FCS (fluorescence correlation spectroscopy) with quenchers present. *J. Phys. Chem. A* **123**, 10184–10189 (2019).

121 Barbotin, A., Galiani, S., Urbančič, I., Eggeling, C. & Booth, M. J. Adaptive optics allows STED-FCS measurements in the cytoplasm of living cells. *Opt. Express* **27**, 23378–23395 (2019).

122 Tsuboi, Y., Shoji, T. & Kitamura, N. Optical trapping of amino acids in aqueous solutions. *J. Phys. Chem. C* **114**, 5589–5593 (2010).

123 Pagès, G., Gilard, V., Martino, R. & Malet-Martino, M. Pulsed-field gradient nuclear magnetic resonance measurements (PFG NMR) for diffusion ordered spectroscopy (DOSY) mapping. *Analyst* **142**, 3771–3796 (2017).

124 Antalek, B. Using pulsed gradient spin echo NMR for chemical mixture analysis: how to obtain optimum results. *Concepts Magn. Reson.* **14**, 225–258 (2002).

125 Kiraly, P., Swan, I., Nilsson, M. & Morris, G. A. Improving accuracy in DOSY and diffusion measurements using triaxial field gradients. *J. Magn. Reson.* **270**, 24–30 (2016).

126 Connell, M. A. et al. Improving the accuracy of pulsed field gradient NMR diffusion experiments: correction for gradient non-uniformity. *J. Magn. Reson.* **198**, 121–131 (2009).

127 Dey, K. K. *et al.* Chemotactic separation of enzymes. *ACS Nano* **8**, 11941–11949 (2014).

128 Karshalev, E., Esteban-Fernández de Ávila, B. & Wang, J. Micromotors for "chemistry-on-the-fly". *J. Am. Chem. Soc.* **140**, 3810–3820 (2018).

129 Singh, V. V., Kaufmann, K., Esteban-Fernández de Ávila, B., Uygun, M. & Wang, J. Nanomotors responsive to nerve-agent vapor plumes. *Chem. Commun.* **52**, 3360–3363 (2016).

130 Li, J. *et al.* Micromotors spontaneously neutralize gastric acid for pH-responsive payload release. *Angew. Chem. Int. Ed.* **56**, 2156–2161 (2017).

131 Esteban-Fernández de Ávila, B. *et al.* Hybrid biomembrane-functionalized nanorobots for concurrent removal of pathogenic bacteria and toxins. *Sci. Robot.* **3**, eaat0485 (2018).

132 Esteban-Fernández de Ávila, B. *et al.* Acoustically propelled nanomotors for intracellular siRNA delivery. *ACS Nano* **10**, 4997–5005 (2016).

133 Joseph, A. *et al.* Chemotactic synthetic vesicles: design and applications in blood–brain barrier crossing. *Sci. Adv.* **3**, e1700362 (2017).

134 Jurado-Sánchez, B. & Wang, J. Micromotors for environmental applications: a review. *Environ. Sci. Nano.* **5**, 1530–1544 (2018).

135 Wang, J., Dong, R., Wu, H., Cai, Y. & Ren, B. A review on artificial micro/nanomotors for cancer-targeted delivery, diagnosis, and therapy. *Nano-Micro Lett.* **12**, 11 (2019).

136 Ou, J. *et al.* Micro/nanomotors toward biomedical applications: the recent progress in biocompatibility. *Small* **16**, 1906184 (2020).

137 Peng, F., Tu, Y. & Wilson, D. A. Micro/nanomotors towards in vivo application: cell, tissue and biofluid. *Chem. Soc. Rev.* **46**, 5289–5310 (2017).

138 Katuri, J., Ma, X., Stanton, M. M. & Sánchez, S. Designing micro- and nanoswimmers for specific applications. *Acc. Chem. Res.* **50**, 2–11 (2017).

139 Li, J., Esteban-Fernández de Ávila, B., Gao, W., Zhang, L. & Wang, J. Micro/nanorobots for biomedicine: delivery, surgery, sensing, and detoxification. *Sci. Robot.* **2**, eaam6431 (2017).

140 Gao, C. Y., Wang, Y., Ye, Z. H., Lin, Z. H., Ma, X., He, Q., Biomedical micro-/nanomotors: from overcoming biological barriers to in vivo imaging. *Adv. Mater.* **33**, 2000512 (2021).

141 Ramaiya, A., Roy, B., Bugiel, M. & Schäffer, E. Kinesin rotates unidirectionally and generates torque while walking on microtubules. *Proc. Natl Acad. Sci. USA* **114**, 10894–10899 (2017).

142 Kinosita, K., Yasuda, R., Noji, H. & Adachi, K. A rotary molecular motor that can work at near 100% efficiency. *Philos. Trans. R. Soc., B* **355**, 473–489 (2000).

143 Sumi, T. & Klumpp, S. Is F_1-ATPase a rotary motor with nearly 100% efficiency? Quantitative analysis of chemomechanical coupling and mechanical slip. *Nano Lett.* **19**, 3370–3378 (2019).

144 Chattopadhyay, S., Moldovan, R., Yeung, C. & Wu, X. L. Swimming efficiency of bacterium *Escherichia coli*. *Proc. Natl Acad. Sci. USA* **103**, 13712–13717 (2006).

145 Wang, W., Chiang, T.-Y., Velegol, D. & Mallouk, T. E. Understanding the efficiency of autonomous nano- and microscale motors. *J. Am. Chem. Soc.* **135**, 10557–10565 (2013).

146 Shah, Z. H. et al. Highly efficient chemically-driven micromotors with controlled snowman-like morphology. *Chem. Commun.* **56**, 15301–15304 (2020).

147 Zhang, L. *et al.* Characterizing the swimming properties of artificial bacterial flagella. *Nano Lett.* **9**, 3663–3667 (2009).

148 Cnossen, A., Kistemaker, J. C. M., Kojima, T. & Feringa, B. L. Structural dynamics

of overcrowded alkene-based molecular motors during thermal isomerization. *J. Org. Chem.* **79**, 927–935 (2014).

149 Solovev, A. A., Mei, Y., Bermúdez Ureña, E., Huang, G. & Schmidt, O. G. Catalytic microtubular jet engines self-propelled by accumulated gas bubbles. *Small* **5**, 1688–1692 (2009).

150 Armstrong, M. J. & Hess, H. The ecology of technology and nanomotors. *ACS Nano* **8**, 4070–4073 (2014).

151 Laskar, A., Shklyaev, O. E. & Balazs, A. C. Self-morphing, chemically driven gears and machines. *Matter* **4**, 600–617 (2021).

[H1] Acknowledgements

Y.Z. acknowledges the startup funds from Beijing Advanced Innovation Center for Soft Matter Science and Engineering at Beijing University of Chemical Technology (BAIC202103). H.H. acknowledges financial support from NSF-DMR grant 1807514.

[H1] Author contributions

All authors contributed equally to the preparation of the manuscript.

[H1] Competing interest statements

The authors declare no competing interests.

[H1] Publisher's note

[H1] ToC blurb

[please insert a ~30 word summary of the Perspective]

Implementing effective chemo-mechanical coupling in the microscopic world is particularly challenging. This Perspective describes recent advances of chemically-powered swimming or diffusion of objects with sizes ranging from the molecular, over the nano-, to the microscale.

Subject terms

Proteins /639/638/92/612

Nanoparticles /639/301/357/354

Physical chemistry /639/638/440

Catalytic mechanisms /639/638/77/885